

# Microscopic perspective on the adsorption isotherm of a heterogeneous surface: Supporting Information

Rogan Carr<sup>α</sup>, Jeffrey R. Comer<sup>α</sup>, Mark D. Ginsberg<sup>β</sup> and Aleksei Aksimentiev<sup>α,γ<sup>1</sup></sup>

<sup>α</sup>Department of Physics, University of Illinois, Urbana, IL

<sup>β</sup>US Army ERDC-CERL, Champaign, IL

<sup>γ</sup>Beckman Institute for Advanced Science and Technology,  
University of Illinois, Urbana, IL

June 30, 2011

<sup>1</sup>corresponding author. Address: 1110 W. Green St., Department of Physics, University of Illinois, Urbana, IL 61801, U.S.A., Tel.: (217)333-6495, Email: aksiment@illinois.edu

## Supporting Methods

**Molecular dynamics simulations.** All molecular dynamics (MD) simulations were performed using the program NAMD,<sup>1</sup> a 1 fs integration time step, particle mesh Ewald (PME) electrostatics,<sup>2</sup> and periodic boundary conditions. Simulations in the NPT ensemble (constant number of particles N, pressure P and temperature T) were performed using a Langevin thermostat<sup>3</sup> and Nosé-Hoover Langevin piston pressure control<sup>4</sup> set at 295 K and 1 atm, respectively. The damping coefficient of the Langevin thermostat was 1 ps<sup>-1</sup> and was applied only to the atoms of the silica surfaces, unless specified otherwise. A smooth (1.0–1.2 nm) cutoff was used to compute the Lennard-Jones forces. External potentials were applied using grid-steered molecular dynamics (G-SMD).<sup>5</sup> All simulations were performed using the TIP3P water model modified for the CHARMM<sup>6</sup> force field and a CHARMM-compatible model for silica,<sup>7</sup> except during membrane generation. In the simulations of solute adsorption, the charges of the silicon and oxygen atoms of silica were set to 0.9  $e$  and  $-0.45 e$ , respectively, and the Lennard-Jones parameters were  $r_{\text{Si}}^{\text{min}} = 0.4295$  nm,  $\epsilon_{\text{Si}} = 0.3$  kcal/mol,  $r_{\text{O}}^{\text{min}} = 0.35$  nm, and  $\epsilon_{\text{O}} = 0.15$  kcal/mol.

**All-atom model for dimethyl methylphosphonate (DMMP).** To model DMMP, we have adapted the united-atom DMMP parameters developed by Vishnyakov and Neimark<sup>8</sup> for use with the CHARMM force field.<sup>6</sup> Tables S1 a–e list the all-atom parameters for DMMP based on the original united-atom model<sup>8</sup> with additions from the CHARMM force field<sup>6</sup> and quantum chemical calculations.<sup>9,10</sup> The parameters for DMMP provided by Vishnyakov and Neimark were not charge neutral. To correct this, we subtracted 0.004  $e$  from the charge of the phosphorus oxygen and 0.002  $e$  from the charge of each methyl carbon, where  $e$  is the charge of a proton. The addition of three hydrogens was performed according to the standard CHARMM parameter protocol. That is, hydrogens were each given a charge of +0.09  $e$ ; this was balanced by subtracting an equal amount of charge from the parent atom. A list of all the atomic charges is given in Table S1 a.

To compare our parameters to those of Vishnyakov and Neimark,<sup>8</sup> we created two test systems of DMMP solvated in TIP3P<sup>11</sup> water at 4.6 and 1.1 mol/L concentrations. The first system recreates “mixture I” in,<sup>8</sup> while the second system tests our model at lower concentration. MD simulations were performed on both systems in the NPT ensemble at 303 K and 1 atm for 10 ns. The parameters of Vishnyakov and Neimark<sup>8</sup> were developed for a 1-4 scaling factor of 0.5, but our model of silica uses a 1-4 scaling factor of 1.0. In order to determine whether our adapted DMMP parameters could be used with a 1-4 scaling factor of 1.0, we performed each simulation twice, once with each 1-4 scaling factor.

Table 2 shows a comparison of the all-atom model with the united-atom model. Like the united-atom DMMP molecules, our all-atom DMMP molecules do not aggregate in solution. To determine the diffusion constant of DMMP in water, we have measured the mean squared displacement (MSD) of the DMMP molecules over all independent 10, 20, 50, 100, 200, 500, 1000, 2000 and 5000 ps periods during our simulations and used weighted linear regression to calculate  $\frac{d}{dt}(\text{MSD})$ . The Einstein relation

$$\langle r^2(t) \rangle = 6Dt$$

or, in terms of the MSD

$$D = \frac{1}{6} \lim_{t \rightarrow \infty} \frac{d}{dt}(\text{MSD}),$$

was used to calculate the diffusion constant. The measured diffusion constant of DMMP in water with our parameters is found to be 13% be greater than DMMP as described by the united-atom parameters at the same concentration. At a concentration of 1.1 mol/L, the diffusivity of DMMP increases by almost a factor of two. Hydrogen bonding between water and the DMMP oxygens was considered using the same metrics as in Vishnyakov and Neimark:<sup>8</sup> A distance cutoff of 3.4 Å and a minimum O-H-O angle of 120 degrees. Our model shows a higher affinity for accepting hydrogen bonds than the united-atom model,<sup>8</sup> but is within the experimental range of 2–3 hydrogen bonds per molecule in pure water.<sup>12</sup> The difference between the results for diffusion and hydrogen bonding is most likely due to the difference in water models. The self-diffusion of TIP3P water used in our simulations is more than twice that of the SPC/E model used in,<sup>8</sup> which leads to quicker diffusion for solutes in our simulations. In addition, the united-atom simulations used rigid SPC/E water, which may have reduced the hydrogen-bonding count. The use of 1-4 scaling of 0.5 or 1.0 had no

measurable effect on the dynamics of DMMP. In accordance with our silica parameters, a 1-4 scaling of 1.0 was used for all further simulations. To test the DMMP parameters at the same temperature and similar concentration to our adsorption chamber simulations, we created a third system at 0.62 mol/L concentration and simulated it in the NPT ensemble for 10 ns at 295 K. The results of this simulation, presented in Table 2, show that the diffusion constant remains the same, while the affinity for accepting hydrogen bonds increases slightly to 2.8 hydrogen bonds per molecule.

Atom	Charge (e)
P*	1.17
O2	-0.695
OS	-0.36
CT3 <sub>P</sub>	-0.291
CT3 <sub>OS</sub>	-0.137
HC3 <sup>∇</sup>	0.09

Bond	Length (Å)	Strength (kcal/mole/Å <sup>2</sup> )
CT3 P	1.795*	1.86 <sup>†</sup>
CT3 HC3 <sup>∇</sup>	322.0	1.111
CT3 OS <sup>∇</sup>	340.0	1.43
OS P <sup>∇</sup>	269.0	1.60
O2 P <sup>∇</sup>	580.0	1.48

Angle	Theta (degrees)	Strength (kcal/mole/Å <sup>2</sup> )	U-B Length (Å)	(U-B) Strength (kcal/mole/Å <sup>2</sup> )
OS P OS <sup>∇</sup>	104.3	80.0		
HC3 CT3 OS <sup>∇</sup>	109.5	60.0		
HC3 CT3 HC3 <sup>∇</sup>	108.40	35.500	5.40	108.40
O2 P CT3*	116.3	80.0		
CT3 P OS*	104.3	40.6		
O2 P OS*	116.5	100.1		
P OS CT3*	121.0	80.0		
P CT3 HC3 <sup>†</sup>	110.0	50.0		

Dihedral	K <sub>χ</sub> (kcal/mole)	n	Δ (degrees)
CT3 P OS CT3*	0.0671	1	0.00
CT3 P OS CT3*	0.6289	2	0.00
CT3 P OS CT3*	0.0755	3	0.00
CT3 P OS CT3*	-0.0582	4	0.00
CT3 P OS CT3*	0.0733	5	0.00
CT3 P OS CT3*	-0.0060	6	0.00
HC3 CT3 P OS*	0.0000	3	0.00
HC3 CT3 P O2*	0.0000	3	0.00
O2 P OS CT3*	0.1004	3	0.00
OS P OS CT3*	0.9536	2	0.00
OS P OS CT3*	0.5019	3	0.00
X CT3 OS X <sup>∇</sup>	0.00	3	0.00

Atom	epsilon	Rmin/2 (Å)
HC3 <sup>∇</sup>	-0.024	1.3400
P*	-0.347	1.192
O2*	-0.159	1.47
CT3*	-0.208	1.90
OS*	-0.159	1.52

Table S1: All-atom, CHARMM-compatible parameters for MD simulations of DMMP. The tables specify (a) charge, (b) bond, (c) angle, (d) dihedral and (e) lennard-jones parameters. The parameters are based on the united-atom model<sup>8</sup> (indicated with an \*), modified in accordance with the CHARMM force field<sup>6</sup>(<sup>∇</sup>) and *ab initio* quantum chemical calculations<sup>9,10</sup> (<sup>†</sup>).

**All-atom model for synthetic surfaces.** To produce the silica membrane used in this study, we created a  $2.5 \times 2.5 \times 3.5$  nm<sup>3</sup> block of crystalline silica containing 500 silicon and 1000 oxygen atoms by replicating a unit cell of SiO<sub>2</sub>. The resulting system was annealed through NVT (constant number of particles N, volume V and temperature T) simulations for 20 ps at 7000 K, 20 ps at 5000 K, 50 ps at 2000 K, 100 ps at 1000 K, and 50 ps at 300 K using the BKS potential<sup>13,14</sup> and a  $2.5 \times 2.5 \times 5.5$  nm<sup>3</sup> periodic cell, to produce an amorphous silica membrane with two relaxed surfaces (normal to the z-axis). As in Vollmayer et al.,<sup>14</sup> the form of the BKS potential was modified at small distances to prevent spurious behavior at high temperature. The Coulomb portion of the BKS potential was computed using the PME method,<sup>2</sup> while the Lennard-Jones portion was smoothly shifted to zero at an interatom distance of 0.55 nm. During the

System	# Atoms	[DMMP], (mol/L)	Duration (ns)	1-4 Scaling	$D$ , $10^{-6}\cdot\text{cm}^2/\text{s}$	# Hydrogen Bonds
UA	1419	4.6	0.5	0.5	4.5	1.7
I	13,728	4.6	9.5	0.5	$5.2 \pm 0.1$	2.2
I	13,728	4.6	10	1.0	$5.0 \pm 0.2$	2.3
II	10,528	1.1	10	0.5	$9.3 \pm 0.2$	2.5
II	10,528	1.1	10	1.0	$9.2 \pm 0.1$	2.5
III	57,296	0.62	10	1.0	$9.1 \pm 0.1$	2.8

Table S2: Comparison of the united-atom (UA) model of DMMP<sup>8</sup> with our all-atom model at three concentrations of DMMP. Simulations of systems I and II were performed using two values of 1-4 scaling: 0.5 and 1.0.

annealing procedure, an external force was applied to prevent the atoms from evaporating into the vacuum region. The temperature was controlled by Langevin dynamics with a damping constant of  $5 \text{ ps}^{-1}$ .

From the results of the annealing simulations, we created four  $\text{SiO}_2$  surfaces, each with different surface properties. Surfaces A and B were generated by removing atoms within 0.42 nm of the top and bottom surfaces from the structure at the end of the annealing process, resulting in two different surfaces that were similar to cross sections of bulk amorphous silica. The resulting structure, having surface A as its bottom surface and surface B as its top surface is referred to as system AB. System A was created by splitting system AB in half and replicating and rigidly transforming the half containing surface A to produce a silica slab having identical surfaces (A) on the top and bottom.

The same replication and transformation procedure was used to produce system C using the bottom half of the  $\text{SiO}_2$  block and the atomic coordinates from the first step of the annealing procedure—20 ps at 700 K. This system had similar properties to the system used in Carr et al.<sup>15</sup> System D was made in the same way as system C except that atomic coordinates from the end of the annealing procedure were used. Thus, the two identical surfaces of system D can be thought of as more relaxed than the two identical surfaces of system C due to the more gradual annealing process in the first case.

The use of the BKS force field in the annealing simulations was to produce plausible atomic structures for the  $\text{SiO}_2$  surfaces. In the subsequent simulations of the adsorption chamber, the  $\text{SiO}_2$  atoms were restrained to the positions generated by the annealing simulations.<sup>7,15,16</sup> The strength of the restraints and bonds were chosen to give the membrane a dielectric constant of  $\sim 5$ . The restraint force was given by  $F(\vec{r}_i) = -2K(\vec{r}_i - \vec{R}_i)$ , where  $\vec{r}_i$  and  $\vec{R}_i$  are the current and initial positions of atom  $i$  and  $K = 13,900 \text{ pN/nm}$ . Bonds were established between all silicon and oxygen atoms separated by  $< 0.22 \text{ nm}$  using with  $K_{\text{bond}} = 695 \text{ pN/nm}$ . The interaction of the  $\text{SiO}_2$  atoms with water and DMMP were calculated using the CHARMM compatible force field of Cruz-Chu et al.<sup>7</sup>

To separate the effects of surface roughness from other surface features, a fifth surface, which we will refer to as the phantom or Ph surface, was used. This surface did not consist of atoms; instead an infinitely smooth, frictionless surface was modeled by applying the following smooth potential to all atoms using G-SMD.<sup>5</sup>

$$U(z) = \begin{cases} U_0 & \text{if } |z| \leq z_0 \\ 0 & \text{if } |z| \geq z_0 + 2l \\ \frac{1}{4}U_0 \left( 2 - 3\frac{|z|-(z_0+l)}{l} + \left(\frac{|z|-(z_0+l)}{l}\right)^3 \right) & \text{otherwise} \end{cases}$$

where  $U_0 = 5 \text{ eV}$ ,  $l = 0.2 \text{ nm}$ , and  $z_0 = 1.25 \text{ nm}$ .

**Solute adsorption simulations and analysis.** The simulations of solute adsorption were performed using atomic-scale models of small chambers that contained DMMP solution enclosed between two surfaces (see Figure 1). Systems A, AB, C and D were created using silica slabs A, AB, C, D, respectively, tiled in a four-by-four grid to create new slabs consisting of sixteen identical patches, measuring  $10 \times 10 \text{ nm}^2$  in total area. System Ph was created using a phantom surface slab (Ph, described above), measuring  $10 \times 10 \text{ nm}^2$  in area. To create the enclosed chambers, the silica or phantom slab was placed in a periodic box with the same width and breadth as the slab, but with a height greater than that of the slab, creating systems that

were effectively infinitely long and wide, with a gap of 5 to 6 nm separating the surfaces (see Figure 1). The volume between the surfaces was then filled with a solution of DMMP.

Surface	Length (ns)	$\Delta P$ (bar)	$N_{\text{DMMP}}$	$n_{\text{DMMP}}$ nm <sup>-2</sup>	$C_{\text{bulk}}$ M
A	100	71.0	25	0.078	0.035
A	100	71.0	50	0.16	0.060
A	100	70.0	100	0.30	0.13
A	100	69.0	150	0.43	0.20
A	100	69.0	200	0.56	0.28
A	50	0.0	200	0.56	0.28
A	100	67.0	300	0.76	0.46
A	100	41.0	1500	1.6	4.6
A <sub>AB</sub>	100	67.0	200	0.67	0.38
B <sub>AB</sub>	100	67.0	200	0.16	0.38
A <sub>AB</sub>	100	41.0	1500	1.6	4.7
B <sub>AB</sub>	100	41.0	1500	0.83	4.7
C	100	63.0	400	1.7	0.17
C	100	41.0	1500	2.3	4.1
D	50	60.0	200	1.0	0.005
D	100	60.0	400	2.0	0.014
D	100	60.0	600	2.3	0.43
D	100	41.0	1500	2.5	4.1
Ph	50	69.0	200	0.26	0.57
Ph	100	41.0	1500	1.5	4.7

Table S3: Summary of solute adsorption simulations. Each simulation is characterized by the duration of the NVT portion of the simulation, the pressure difference across the chamber ( $\Delta P$ ), the total number of DMMP molecules ( $N_{\text{DMMP}}$ ), the steady-state adsorption density ( $n_{\text{DMMP}}$ ) and the steady-state bulk concentration  $C_{\text{bulk}}$  (see Figure 1). Each simulation of system AB, which contained both surfaces A and B, is listed twice, specifying adsorption densities for individual surfaces, labeled A<sub>AB</sub> and B<sub>AB</sub>.

Following a 2000-step minimization using a conjugate gradients method, each system was equilibrated for 1.5 ns in the NPAT ensemble (constant number of particles N, pressure P, area in the  $xy$  plane A and temperature T). During the NPAT simulation, some DMMP molecules may have adsorbed to the surfaces. To remove this effect, all DMMP molecules were moved back to their initial coordinates, and constrained to those coordinates for a 0.5 ns simulation in the NVT ensemble, removing any steric clashes between DMMP and water molecules. Each system was then simulated in the NVT ensemble with a pressure gradient induced in the  $x$ -direction, resulting in a pressure-driven flow of DMMP solution through the system. To induce a pressure gradient, a constant force in the  $x$ -direction  $F_x$  was applied to all  $N$  water molecules, creating a pressure difference  $\Delta P_x$  across the system of

$$\Delta P_x = N \cdot F_x / A, \tag{1}$$

where  $A$  is the area of the chamber in the  $yz$  plane.<sup>15</sup> Temperature was maintained by applying the Langevin thermostat to all silica atoms, which was sufficient to keep the temperature of the entire system within 1.2% of the target temperature.<sup>15</sup> To investigate whether the pressure-driven flow affected the amount of solute bound, we performed simulations of system A with and without the applied pressure difference, which showed that the pressure-driven flow had no measurable effect on adsorption. A summary of all solute adsorption simulations is given in Table 3. For all simulations of the phantom channel, the Langevin temperature control was applied only to water oxygens with a damping coefficient of 0.1 ps<sup>-1</sup>.

To calculate the solute adsorption densities at the surfaces, a DMMP molecule was considered adsorbed if its phosphorus atom, approximately the center of mass, was within 0.5 nm of the surface. The surface of each silica slab was defined as the  $x - y$  plane with the  $z$  coordinate determined as the average  $z$  coordinate of the isosurface defined by the five-to-one ratio of silica and water atoms. The region extending 0.5 nm away from that surface is referred to as the adsorption layer, see Figure 1. The average solute adsorption densities were calculated by removing data before 15 ns, keeping only steady-state data. Figure S1 shows a

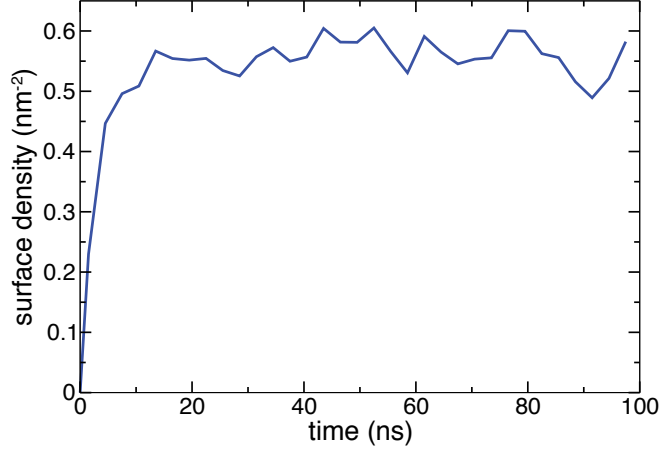


Figure S1: The surface density of adsorbed DMMP as a function of time in system A, block averaged in 3-ns intervals.

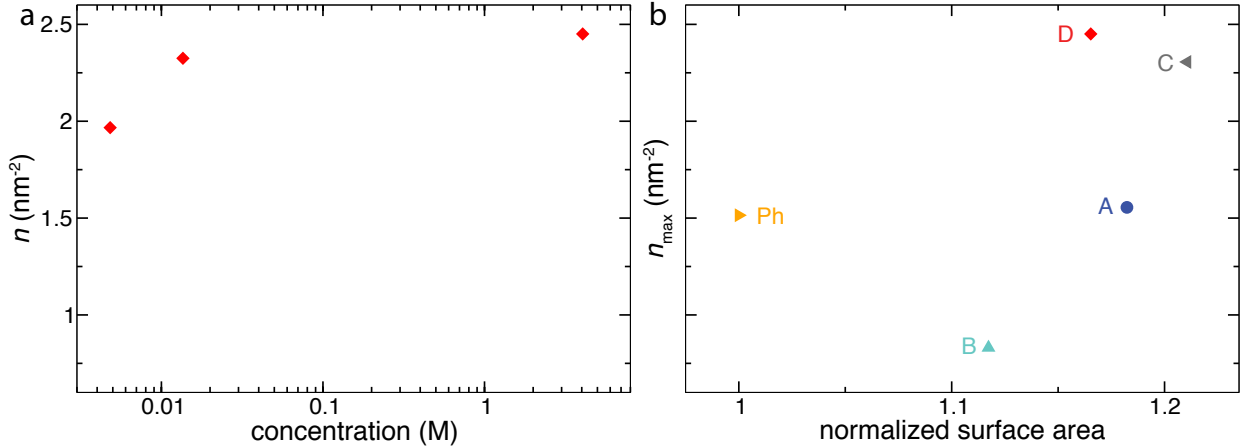


Figure S2: Calculations of the maximum adsorption density  $n_{\max}$ . a) Surface density of DMMP as a function of DMMP bulk concentration for system D. b) The maximum adsorption density  $n_{\max}$  as a function of the normalized surface area for each surface studied (see text).

typical plot of the surface density of adsorbed DMMP as a function of time. The system reaches a steady state in 15 ns.

**Calculations of the maximum adsorption density.** The maximum adsorption density  $n_{\max}$  was computed for each surface and was found to depend on its atomic-scale features. To determine  $n_{\max}$ , we used the expression for the Langmuir isotherm in terms of the adsorption densities,

$$n = n_{\max} \frac{\alpha C_{\text{bulk}}}{1 + \alpha C_{\text{bulk}}}. \quad (2)$$

In the limit of high concentration, the surface density  $n$  asymptotically approaches  $n_{\max}$ . To determine  $n_{\max}$ , we performed brute-force simulations of DMMP adsorption in system D for a range of DMMP concentrations. The resulting dependence of surface density on bulk concentration is shown in Figure S2 a. As the bulk concentration increased, the adsorption density approached a constant value. Thus, we chose  $n_{\max}$  for surface D to be the adsorption density at the highest bulk concentration simulated, which was 4.1 M. As surface D has the highest affinity to DMMP of all surfaces considered, to determine  $n_{\max}$  for the other four surfaces (A, B, C and Ph), we simulated systems A, AB, C and Ph at the same initial DMMP concentration

as the one that yielded  $n_{\max}$  for system D. The simulation of system AB was used to determine  $n_{\max}$  for surface B. To verify that the presence of two surfaces (A and B) in one simulation did not affect the determination of  $n_{\max}$ , we compare the value of  $n_{\max}$  for surface A calculated through simulation of system A with that calculated through simulation of system AB. The value of  $n_{\max}$  for surface A in system AB at 4.7 M: 1.7 molecules/nm<sup>-1</sup> agreed with the value in system A at 4.6 M: 1.7 molecules/nm<sup>-1</sup>.

The value of  $n_{\max}$  for each surface is shown in Figure S2 b, plotted as a function of the normalized surface area. The normalized surface area was calculated as the solvent-accessible surface area (SASA) divided by the planar ( $x - y$  plane) area of the slab. To calculate the SASA, we used the ‘measure sasa’ feature of the Visual Molecular Dynamics (VMD)<sup>17</sup> package, using a solvent radius of 1.4, the approximate radius of a water molecule. Figure S2 b shows that  $n_{\max}$  is not a simple geometric parameter. Approximating a DMMP molecule as a disk of radius 0.23 nm (the radius of gyration) that packs in a hexagonal lattice with a packing density of 0.9069, one would expect  $n_{\max}$  to correspond to a density of  $\sim 5.6$  molecules nm<sup>-2</sup>. However, the observed maximum adsorption densities are much lower and depend on the properties of individual surfaces. Furthermore, Figure S2 b shows that  $n_{\max}$  is not a function of the normalized surface area, meaning that variation in  $n_{\max}$  is not caused by the variation in the surface area of the slabs, even after taking into account the atomic scale roughness.

**Umbrella sampling simulations.** To study the interaction between a single DMMP and the membrane surfaces, we created 5 small systems consisting of a single slab of silica membrane or an equal size phantom membrane, water, and one DMMP molecule. The potential of mean force (PMF) of a DMMP molecule as a function of its position relative to the membrane surface was determined from a set of umbrella sampling simulations,<sup>18</sup> which were analyzed using the weighted histogram analysis method (WHAM)<sup>19</sup> generalized to three dimensions (see below). Prior to the umbrella sampling simulations, each of the four systems underwent 2000 steps of energy minimization, 2 ps of equilibration at fixed volume during which the temperature was raised from 0 to 295 K by velocity rescaling, and 200 ps of NPT simulation.

The umbrella sampling simulations were performed by restraining the phosphorus atom of the DMMP molecule to points in  $(x, y, z)$  (where  $z$  is perpendicular to the surface) using the potential energy function  $w_i(x, y, z) = \frac{1}{2}k_x(x - x_i)^2 + \frac{1}{2}k_y(y - y_i)^2 + \frac{1}{2}k_z(z - z_i)^2$ , where  $(x_i, y_i, z_i)$  was the center of sampling window  $i$  and  $k_x$ ,  $k_y$  and  $k_z$  were the spring constants along each axis. Because the gradient of the PMF was much larger along the  $z$  axis than in the  $xy$  plane, a stiffer spring constant of  $k_z = 1390$  pN/nm was used along the  $z$  axis than perpendicular to it, for which  $k_x = k_y = 70$  pN/nm. Furthermore, the sampling windows  $(x_i, y_i, z_i)$  were more closely spaced along the  $z$  axis. The sampling windows formed a three-dimensional grid with 4, 4, and 9 points along the  $x$ ,  $y$ , and  $z$  directions, respectively. Results were first obtained using the 144 sampling windows centered at these points, but to increase the resolution of our PMF distributions, we added another 300 sampling windows. For these simulations, we used a grid of 5, 5, and 12 points with spring constants  $k_x = k_y = 560$  and  $k_z = 2780$  pN/nm. To ensure that the calculated PMF extended into bulk water, 19 sampling windows with the same spring constant as the previous set were added to the  $(x, y)$  center of the slab for an additional nanometer in  $z$ . Each simulation represented more than 2.2 ns. The first 0.2 ns of each simulation was excluded from the WHAM PMF calculation.

**Potential of mean force calculation.** The potential of mean force (PMF) is computed by the weighted histogram analysis method (WHAM) described by Roux<sup>19</sup> generalized to three dimensions. Each of the three spatial dimensions is a reaction coordinate. We estimate the unbiased probability distribution by

$$\langle \rho(x, y, z) \rangle = \left( \sum_{i=1}^{N_w} n_i \langle \rho_i(x, y, z) \rangle \right) \left( \sum_{j=1}^{N_w} n_j \exp \left[ -\frac{w_j(x, y, z) - F_j}{k_B T} \right] \right)^{-1}, \quad (3)$$

where  $\rho(x, y, z)$  is the unbiased probability distribution,  $N_w$  is the number of biased simulations,  $\rho_i(x, y, z)$  is the biased probability distribution derived from the results of biased simulation  $i$ ,  $n_i$  and  $w_i(x, y, z)$  are the number of independent data points and the biasing potential, respectively, for biased simulation  $i$ , and  $\{F_i\}$  is a set of constants.

The set of constants  $\{F_i\}$  are initially unknown; thus, we make an initial guess for their values. After estimating  $\langle\rho(x, y, z)\rangle$  by Equation 3, we can obtain improved estimates these constants by solving

$$\exp\left[-\frac{F_i}{k_B T}\right] = \int dx \int dy \int dz \exp\left[-\frac{w_i(x, y, z)}{k_B T}\right] \langle\rho(x, y, z)\rangle. \quad (4)$$

To obtain self-consistency, the equations are iterated, feeding the newest estimate of  $\{F_i\}$  into Equation 3 and then the newest estimate of  $\langle\rho(x, y, z)\rangle$  into Equation 4. Iteration ceases at iteration  $j$  when  $|(F_{i+1} - F_i)^{(j)} - (F_{i+1} - F_i)^{(j-1)}| < 0.0001 k_B T$  for all windows  $i \in \{1, 2, \dots, N_w - 1\}$ . The PMF is then computed by  $-k_B T \log(\langle\rho(x, y, z)\rangle)$ .

**Surface Characterization.** To characterize the atomic-scale features of the surfaces, we computed the local surface roughness and the local surface charge density of each surface. Topographical maps of the surfaces, shown in Figure S3, were generated using hard spheres with radii of 0.2 nm as probes and considering the silicon and oxygen atoms as hard spheres with radii of 0.2147 nm and 0.175 nm, respectively. To compare the surfaces, the reference height  $z = 0$  was defined to be the mean value of  $z$  (direction normal to the plane of the slab) over the topographical map of that surface. The the root-mean-square (RMS) roughness for each surface was then computed from the topographical maps. In Figure S4, the Langmuir constant for each surface is shown as a function of its RMS roughness.

The surface charge density for each surface was computed using the ‘volmap’ tool in Visual Molecular Dynamics (VMD).<sup>17</sup> To compute the surface charge density, the charge of each atom comprising the silica slab was distributed over a three-dimensional grid of 0.42 Å resolution by approximating each atom as a normalized Gaussian distribution with width equal to the radius of the atom and taking into account the periodicity of the system. The resulting three-dimensional grid, periodic in  $x$  and  $y$ , described the charge density in the system produced by the silica atoms. Following that, we defined a surface charge layer as the volume above the plane located 2 Å below the silica surface (defined in “Solute adsorption simulations and analysis” of the Supporting Information). The local surface charge density, shown in the bottom row of Figure S3, was calculated as the total charge density of the surface layer at each (x,y) coordinate. In Figure S5, the Langmuir constant is shown as a function of the total surface charge of each silica surface. We found the plot of the Langmuir constant versus the total surface charge to sensitively depend on the definition of the surface charge layer, in contrast to the dependence of the Langmuir constant on the RMS charge density, Figure 5a, which was robust with respect to the definition of the surface charge layer.

## References

- [1] Phillips, J. C.; Braun, R.; Wang, W.; Gumbart, J.; Tajkhorshid, E.; Villa, E.; Chipot, C.; Skeel, R. D.; Kale, L.; Schulten, K. Scalable Molecular Dynamics with NAMD. *J. Comp. Chem.* **2005**, *26*, 1781–1802.
- [2] Batcho, P. F.; Case, D. A.; Schlick, T. Optimized particle-mesh Ewald/multiple-time step integration for molecular dynamics simulations. *J. Chem. Phys.* **2001**, *115*, 4003–4018.
- [3] Brünger, A. T. X-PLOR, Version 3.1: A System for X-ray Crystallography and NMR. The Howard Hughes Medical Institute and Department of Molecular Biophysics and Biochemistry, Yale University, 1992.
- [4] Martyna, G. J.; Tobias, D. J.; Klein, M. L. Constant Pressure Molecular Dynamics Algorithms. *J. Chem. Phys.* **1994**, *101*, 4177–4189.
- [5] Wells, D. B.; Abramkina, V.; Aksimentiev, A. Exploring transmembrane transport through  $\alpha$ -hemolysin with Grid-Steered Molecular Dynamics. *J. Chem. Phys.* **2007**, *127*, 125101.
- [6] MacKerell, A. D., Jr. et al. All-atom empirical potential for molecular modeling and dynamics studies of proteins. *J. Phys. Chem. B* **1998**, *102*, 3586–3616.
- [7] Cruz-Chu, E. R.; Aksimentiev, A.; Schulten, K. Water-Silica force field for simulating nanodevices. *J. Phys. Chem. B* **2006**, *110*, 21497–21508.

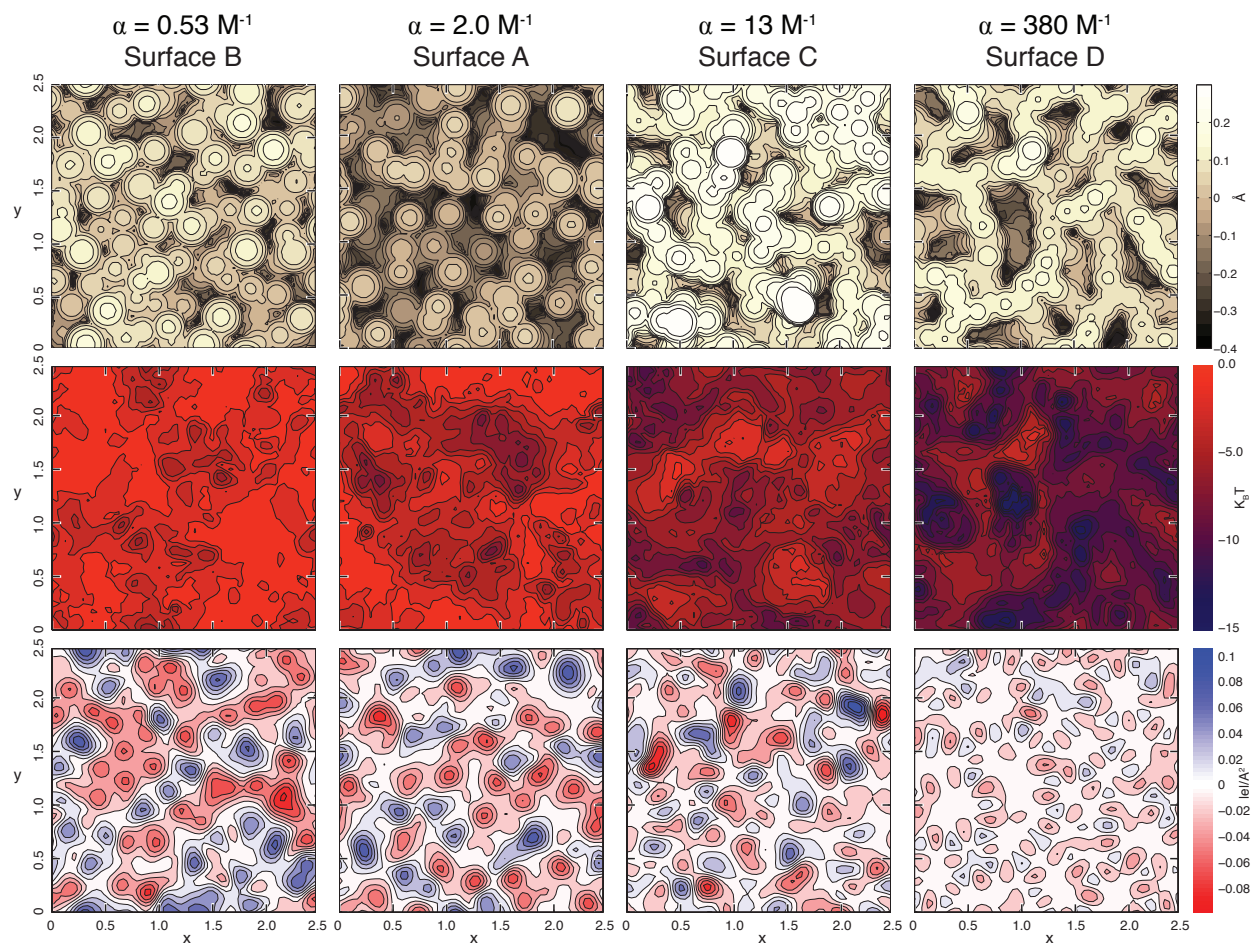


Figure S3: Comparison of the atomic-scale features of the silica surfaces, ordered by increasing Langmuir constant. The surface features are shown on a two-dimensional grid with a resolution of 0.42 Å. (Top row) Topography of each surface, where  $z=0$  is the mean value of  $z$  for that individual surface. (Middle row) Two-dimensional projection of the PMF minima. At each  $(x,y)$  point, the minimum value of the PMF along the line normal to the  $x - y$  plane is shown. (Bottom row) The local charge density of the silica surfaces averaged over the respective MD trajectories (see text).

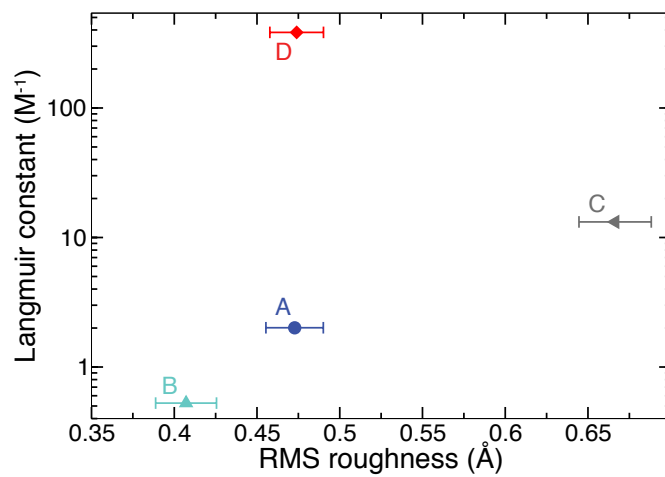


Figure S4: The Langmuir constant as a function of the root mean square (RMS) roughness of the surface.

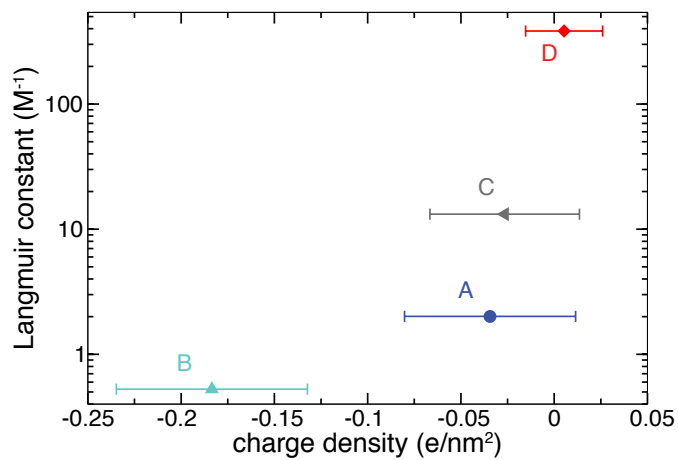


Figure S5: The Langmuir constant as a function of the total charge density of the surface.

- [8] Vishnyakov, A.; Neimark, A. Molecular Model of Dimethylmethylphosphonate and Its Interactions with Water. *J. Phys. Chem. A* **2004**, *108*, 1435–1439.
- [9] Barvik, Jr., I.; Stepanek, J.; Bok, J. Explicit solvent molecular dynamics simulation of duplex formed by the modified oligonucleotide with alternating phosphate/phosphonate internucleoside linkages and its natural counterpart. *J. Biomol. Struct. Dyn.* **2002**, *19*, 863–75.
- [10] Štrajbl, M.; Baumruk, V.; Florián, J.; Bednářová, L.; Rosenberg, I.; Štěpánek, J. Vibrational spectra and quantum mechanical force fields of modified oligonucleotide linkages: 1. methyl methoxymethanphosphonate. *Journal of Molecular Structure* **1997**, *415*, 161 – 177.
- [11] Jorgensen, W. L.; Chandrasekhar, J.; Madura, J. D.; Impey, R. W.; Klein, M. L. Comparison of Simple Potential Functions for Simulating Liquid Water. *J. Chem. Phys.* **1983**, *79*, 926–935.
- [12] Eaton, G.; Harris, L.; Patel, K.; Symons, M. Infrared and nuclear magnetic resonance spectroscopic studies on the solvation of trimethylphosphate and dimethylmethylphosphonate. *Journal of the Chemical Society. Faraday transactions* **1992**, *88*, 3527–3531.
- [13] van Beest, B. W. H.; Kramer, G. J.; van Santen, R. A. Force Fields for Silicas and Aluminophosphates Based on *Ab Initio* Calculations. *Phys. Rev. Lett.* **1990**, *64*, 1955–1958.
- [14] Vollmayr, K.; Kob, W.; Binder, K. Cooling-rate effects in amorphous silica: A computer-simulation study. *Phys. Rev. B* **1996**, *54*, 15808–15827.
- [15] Carr, R.; Comer, J.; Ginsberg, M. D.; Aksimentiev, A. Modeling Pressure-Driven Transport of Proteins through a Nanochannel. *IEEE Tran. Nanotechnol.* **2011**, *10*, 75–82.
- [16] Comer, J.; Wells, D. B.; Aksimentiev, A. *Protocols in DNA nanotechnology*; Humana Press, 2011.
- [17] Humphrey, W.; Dalke, A.; Schulten, K. VMD – Visual Molecular Dynamics. *J. Mol. Graphics* **1996**, *14*, 33–38.
- [18] Torrie, G.; Valleau, J. Nonphysical sampling distributions in Monte Carlo free-energy estimation: umbrella sampling. *Journal of Computational Physics* **1977**, *23*, 187–199.
- [19] Roux, B. The calculation of the potential of mean force using computer simulations. *Computer Physics Communications* **1995**, *91*, 275–282.